Arch. Metall. Mater. **67** (2022), 4, 1387-1394

DOI: https://doi.org/10.24425/amm.2022.141066

HALIL AHMET GÖREN[1*], MEHMET ÜNAL[2], YUNUS TÜREN[3],
HAYRETTIN AHLATÇI[3], YAVUZ SUN[3]

A COMPARATIVE STUDY ON THE MECHANICAL AND CORROSION PROPERTIES OF THE ZM20 AND ZM21 ALLOYS AFTER CASTING AND ROLLING

In this study, the effects of grain refinement and production methods on the corrosion, corrosive wear and mechanical properties of the as-cast and as-rolled Mg-2 wt.% Zn (ZM20) and Mg-2 wt.% Zn-0,51 wt.% Mn (ZM21) alloys were examined by using OM, XRD, SEM, hardness and uniaxial tensile test. Additionally, the potentiodynamic polarization, immersion corrosion test and corrosive wear properties of the ZM20 and ZM21 alloys were compared. According to the XRD results, MgZn and $MgZn_2$ phases were found in the alloys and also $MnZn_3$ phase occurred in the ZM21 alloy with the addition of manganese. Both during solidification forming nucleation points with the added manganese and during rolling the broken secondary phase particles distributed into the matrix prevented grain growth and led to the formation of a more refined structure. The tensile test results showed that the strength of the as-cast ZM21 alloys were better than that of the as-cast ZM20 alloys and further improvement in mechanical properties occurred with the rolling of the both alloys. The most superior hardness was found in the as-rolled ZM21 alloy. In the total 400-m reciprocal corrosive wear test in the 3.5% NaCl solution, the lowest mass loss was in the as-rolled ZM21 alloys. In the potentiodynamic corrosion test, the highest corrosion resistance was occurred by the as-cast ZM20 alloy.

Keywords: Grain size; Hall-Petch relationship; yield stress; corrosion; magnesium

1. Introduction

Mg alloys have received the interest of many researchers in the 21st century to improve energy efficiency and protect the environment. This reveals the importance of Mg alloys as an engineering material. ZM21 is a member of the MgZn alloy system with a low alloy element [1-5]. The usage of unalloyed magnesium as a structural material is not very prevalent due to its low mechanical properties. However, the alloy group with the abbreviation ZM based on the main alloy elements of Mg-Zn-Mn represents a group of desirable properties such as high fracture strength, easy castability and good corrosion resistance [6]. The alloy element Zn plays a significant role in the solid solution and precipitation hardening. Mn addition contributes to grain refining and improvement of corrosion resistance [7]. G. Mann et al. [8], examined the plastic stress in Mg-2Zn casts with grain sized varying between 55 and 340 µm. It is well-known that grain size and yield strength have an inverse relationship, and this relationship is defined with the Hall-Petch equation. In this equation (1), σ_y is the yield strength of the material, σ_f is the frictional strength, k is the material-specific strength constant, and d is the mean grain size of the material [9].

$$\sigma_y = \sigma_f + kd^{-1/2} \tag{1}$$

A reduction in the grain size leads to an increase in the yield strength as a consequence of the increasing grain borders that could counter the dislocation motion [8,10]. While C.H. Caceres et al. [10], they stated that the grain size refinement is inconsistent especially in large grain sizes, G. Mann et al. [8] reported that with the increase of Zr in Mg-2Zn alloy, the grain size becomes finer, and with this, both k and σ_f values increase.

In the study of G. Mann et al. [8], the grain size was above 55 µm due to the grain refinement by adding Zr to the Mg-2Zn alloy produced by sand casting method. The difference of this study from other studies in the literature [7-10] is that the effect of both rolling and Mn addition to Mg-2Zn alloy on grain size, k and σ_f values was investigated in order to reduce the particle size of the Mg-2Zn alloy below 55 µm. To understand the correlation between grain refining and structure-property, the experimental ZM20 and ZM21 magnesium alloys were selected.

[1] SINOP UNIVERSITY, THE VOCATIONAL SCHOOL, MECHATRONIC DEPARTMENT, SINOP, TURKEY
[2] KARABUK UNIVERSITY, MANUFACTURING ENGINEERING, TURKEY
[3] KARABUK UNIVERSITY, METALLURGY AND MATERIALS ENGINEERING, TURKEY

* Corresponding author: agoren@sinop.edu.tr

Therefore; The aim of this study was to compare mechanical properties and corrosion behaviour of ZM20 and ZM21 alloys produced by both casting and rolling.

2. Materials and Methods

In the experiments, in preparation of the ZM20 and ZM21 alloys, commercially magnesium with (~99.9 wt.%) purity support from Bilginoğlu Industrial Materials Industry and Trade Inc., pure Zn (~99.9 wt.%) and Mg−10 wt.% Mn master alloys were used. An atmosphere-controlled induction furnace was used in the melting and casting processes of the alloys. The investigated alloys casted at 750°C, while the mould temperature was set as 250°C. The casting was carried out inside a permanent mould under gas protection (CO_2 (99 vol%) +SF6 (1 vol%)). The chemical compositions of the casted alloys were determined by using a Rigaku ZSX Primus II brand XRF (X-ray fluorescence) device. The chemical compositions of the alloys are given in TABLE 1.

TABLE 1

Chemical compositions of the alloys

Alloys	Elements (wt. %)					
	Zn	Mn	Al	Si	Ca	Mg
ZM20	1.99	0.01	0.02	0.02	0.01	Balance
ZM21	2.05	0.51	0.02	0.01	0.03	Balance

Before the hot rolling process, to prevent defects such as segregation and heterogenous grain sizes that could occur in the cast parts, the cast ZM20 and ZM21 alloys were subjected to homogenization annealing at 400°C for 16 h. Afterwards, following preparation of the specimens at dimensions of 10×30×60 mm, they were rolled with an 80% rolling ratio, 4.7 strain rate and by applying $\varphi = 0.2$ constant deformation degree. $\varphi = -\ln(h_{n+1} / h_n)$, and here, n is the count of passes, and h_n is the specimen thickness after the pass. The specimens were heated to suitable temperatures (350°C) for 60 minutes in a furnace. After each pass was completed, to prevent temperature loss before the next pass started, the specimens were heated back to 350°C for approximately 15 min in accordance with Ref [11].

For microstructure examination the cast and rolled specimens were abraded with respectively 400, 600, 800, 1200 and 2000-mesh sandpapers by using distilled water. Afterwards, the surfaces were polished by using 1 μm alumina. The specimens were then etched with a mixture of 6 g picric acid, 5ml acetic acid, 10 ml distilled water and 100 ml ethanol. The microstructural analyses were carried out with a Nikon optical microscope (OM), SEM images and EDX analyses. In this study, the approximate grain sizes of the ZM20 and ZM21 alloys were determined by utilizing intersections along a 45° test line. At least 500 grains covered by the intersecting line were counted for each specimen. After counting the grains, the total length of the intersecting lines was recorded, and to determine the mean grain size, the intersecting line was divided by the number of the covered grains [12]. After making the counts of the grains covered by lines drawn by an angle of 45° on the optical microscope (OM) images of all specimens with the same magnification rate (100 X) by staying loyal to the grain counting method, and determining the n values as the numbers of grains covered by the obtained measurement line, by applying the value of σ = grain size of the relevant phase, L = total length of the measurement line and n = number of grains covered by the measurement line in the formula, the grain sizes of the specimens were determined in units of μm by an approximate amount. Grain sizes were calculated according to the equation (2) [12].

$$\sigma = L/n \tag{2}$$

The XRD profiles of all cast specimens were obtained with a Rigaku Ultima IV device in the scanning 2θ angle range of 10°-90°, at a scanning rate of 3°/min and using CuKα radiation. The tensile tests of the specimens were carried out with a Zwick/Roell Z600 tensile device at a rate of 1.67×10^{-3} s^{-1} after casting and rolling. The dog-bone tensile specimens with a diameter of 5 mm and gauge length of 25 mm were machined as per EN ISO 6892-1 from the as-cast alloys while the tensile specimens of the as-rolled alloys were prepared along the rolling directions as per ASTM E8 M-04. Each test condition was repeated at least three times.

The hardness values of the specimens were obtained by a Vickers hardness test by using a load of 0.3 kg. The hardness was evaluated by at least 5 hardness measurements. Grain sizes of all specimens were measured with the method of linear intersection with a 45° angle [12]. Characterization of the corrosion properties of the cast and rolled specimens was carried out in a saltwater solution prepared with 3.5% salt (NaCl). The immersion test specimens were taken out of the cast and rolled parts as approximately 2×10×10 mm^3, their surfaces were abraded, and they were cleaned with distilled water in an ultrasonic bath. After calculating the surface areas of the specimens and measuring their initial weight before immersion with a precision scale with a sensitivity of 0.1 mg, the specimens were immerged in a 3.5% NaCl solution put into glass beakers. The immerged specimens were removed from the solution at intervals of 3, 6, and 12 h, and this process continued until the 72 h of treatment time was completed. The corrosion products forming on the surface at each interval were cleaned by keeping the specimens in a chromic acid solution, distilled water and alcohol for 10, 5 and 5 min respectively. The chromic acid solution was prepared inside distilled water at 180 g/L.

The specimens were embedded into epoxy resin after being wrapped in copper wire. After the surface to be tested was abraded and cleaned, a strong adhesive tape with a round hole with an area of 0.25 cm^2 was attached onto the specimen surface, and as a result, the corrosion tests of all specimens were conducted at an equal area, and negative effects that could occur on the corrosion test from the epoxy connection zones were eliminated. The potentiodynamic polarization tests were carried out with a Gamry model PC4/300 mA potentiostat/galvanostat equipped with computer-controlled DC105 corrosion analysis at

room temperature and inside a 3.5% NaCl solution. A classical three-electrode cell was used, where the counter electrode was a graphite rod, the reference electrode was a saturated calomel electrode (SCE), and the working electrode was the specimen surface. Polarization curves were created by scanning at a scanning rate of 1 $mV.s^{-1}$ between –0,25 V (versus open circuit potential, Eoc) and +0,25 V (versus Eoc).

The wear tests of the casting and rolling specimens were carried out with a reciprocal wear test device, in 3.5% NaCl solution. The tests were conducted under 20N load, at 0.1 m/s sliding rate and in a total of 400 m sliding distance. After each wear process of 100 m inside saltwater, the specimen was dried, and the 3.5% NaCl solution in the wear container was replaced. This process was repeated 4 times. The mass losses of the specimens were calculated based on their initial and final weights.

3. Results and discussion

3.1. XRD patterns

Fig. 1 shows the XRD models of the ZM20 alloy. The ZM20 alloy profile consisted of the αMg, MgZn and $MgZn_2$ binary phases. In ZM21 with 0,51 wt.% manganese addition, the $MnZn_3$ binary phase was also observed in addition to these phases. When the diffraction peaks of the ZM21 alloy where this phase emerged were compared to the diffraction peaks of the ZM20 alloy, the peak points at ~48° and ~69° increased in the ZM21 alloy, whereas the peak point at ~58º decreased. It was seen that this situation was related to the formation of the $MnZn_3$ binary phase.

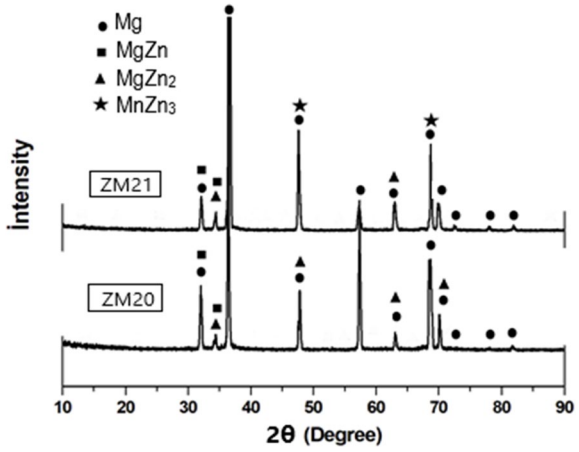

Fig. 1. XRD patterns of the alloys

3.2. Microstructure

The α-Mg mean grain sizes of the cast and rolled alloys are shown micrographs in Fig. 2. The grain size of the ZM21 rolled alloys decreased by approximately 12 µm in comparison to the cast alloys. This decrease from the cast to the rolled form in the ZM20 alloy was 36 µm. While there was an approximately 20 µm difference between the ZM21 and ZM20 alloys in the cast specimens, this difference in the rolled microstructure decreased down to approximately 5 µm. The ZM21 alloy with Mn content of approximately 0,51 wt.%, showed a finer grain size in both the cast and rolled in comparison to the ZM20 alloy.

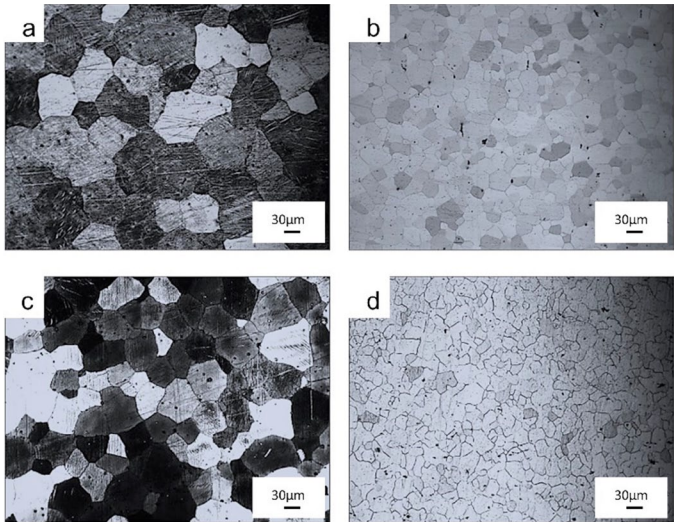

Fig. 2. Optical micrographs of the alloys: (a) as-cast ZM20, (b) as-rolled ZM20, (c) as-cast ZM21 and (d) as-rolled ZM21

Fig. 3 presents the as-cast SEM images and point EDX analysis results taken from the matrix (A and D) and five different secondary phases. As seen in Fig. 1, it is probably considered to be the MgZn and $MgZn_2$ binary phases (B, C, E and F) and the $MnZn_3$ binary phase (G) in the microstructures of the investigated alloys. J. Yan et al. [13], in accord with this study, while the presence of MgZn and $MgZn_2$ phases was reported, no study was found on the presence of $MnZn_3$ intermetallic phase.

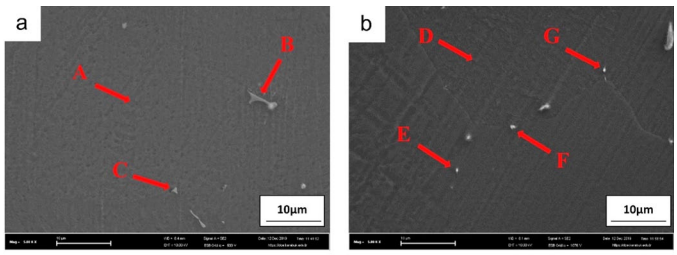

c

Points	Mass percentage (%) Mg	Zn	Mn
A	96.13	3.87	-
B	94.54	5.46	-
C	94.30	5.70	-
D	93.36	6.47	0.18
E	92.08	7.41	0.51
F	79.89	19.82	0.29
G	90.24	5.96	3.80

Fig. 3. SEM micrographs of the as-cast alloys: (a) ZM20, (b) ZM21 and (c) EDX results

3.3. Hardness

Fig. 4 shows the hardness values of the alloys. Among the studied alloys, the lowest hardness value was in the cast ZM20

alloy, while the highest hardness value was in the rolled ZM21 alloy. The hardness values of the as-cast and as-rolled specimens of ZM20 were found respectively as 41, and 49.5 (HV), while that of ZM21 were respectively 43.4 and 57.5 (HV). The increase in hardness is probably due to the presence of intermetallic phases being formed, the refining of the grain size after rolling and the increase in the count of grain boundaries. J. Kubásek and D. Vojtěch [14] reported that the increase in the volume of secondary phases with concentrations of Zn and Gd, improved the hardness with the elements added to pure magnesium.

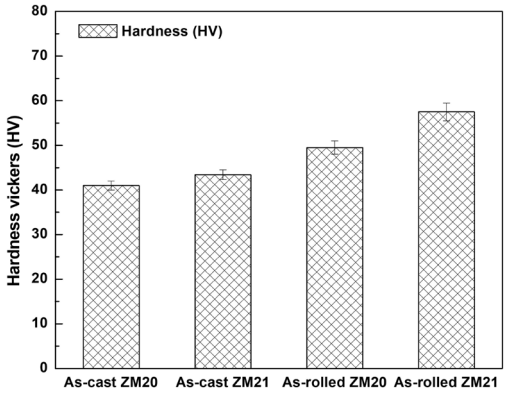

Fig. 4. Hardness results of ZM20 and ZM21 alloys

3.4. Tensile properties

Fig. 5(a) and (b) shows the strength results of the alloys. In accordance with hardness results (Fig. 4) the results of the tensile tests seen in Fig. 5(a) and (b) show that ZM21 was superior to ZM20, and the rolled specimens of both alloys had superior tensile properties. The ultimate strength, yield strength and elongation of the cast ZM20 alloy were respectively 135 MPa, 86 MPa and 3.4%, while these values for its rolled specimens were respectively 261.5 MPa, 130 MPa and 13%. The ultimate strength, yield strength and elongation of the cast ZM21 alloy were respectively 170 MPa, 96 MPa and 5.6%, while these values for its rolled specimens were respectively 270 MPa, 140.2 MPa and 17%. Phase particles broken and dispersed into the matrix during rolling prevented grain largening and caused a more refined structure. G. Mann et al. [8], determined the plastic stress in Mg-2Zn casts with grain sizes varying between approximately 55 and 340 μm.

The k and σ_f values of the investigated alloys are shown in TABLE 2. G. Mann et al. [8], reported that with the increase of Zr content in Mg-2Zn alloy, the grain size became finer and both k and σ_f values increased. In the present study investigated the effect of up to 0,51 wt.% Mn addition to Mg-2Zn alloy on the grain sizes, k and σ_f values given for the as-cast and as-rolled conditions (TABLE 2) were found to increase with production methods. The higher σ_f value with the increase in the number of grain sizes of the as-rolled alloys compared to that of the as-cast alloys can be attributed to the increase in lattice resistance. C.H. Caceres et al. [10] stated that with increasing Zn concentration, the Hall-Petch stress density factor k increased, and the k values range from (~0.28 MPa $m^{1/2}$) for pure Mg and (~0.7 MPa $m^{1/2}$) for (2.3 wt.%) Zn alloy. However, in the case of Mg and its alloys shows large discrepancies in the values of both k and σ_f.

I.T. Caraballo et al. [15] reviewed the Hall-Petch relationship on solid-solution strengthening of Mg alloy and modelled employing a power-law approach. Grain refinement effects were described employing thermodynamic and kinetic formulations via the interdependence theory approach. I.T. Caraballo and P.E.J.R.D.D. Castillo [9] reported that k and σ_f values were influenced in a complex way by the composition, the critical resolved shear stress, thermo-mechanical process parameters of Mg alloys and still remain uncertain.

TABLE 2

The σ_f and k value of the investigated alloys

Alloy	σ_f(MPa)	k (MPam$^{1/2}$)
The as-cast conditions	15,90	1,11
The as-rolled conditions	17,40	1,08

3.5. Corrosion behaviour

3.5.1. Immersion tests

The time-dependent mass losses in the immersion corrosion test are shown in Fig. 6. As seen in Fig. 6(a), mass loss per unit area versus time changed linearly. The as-rolled ZM21 exhibited

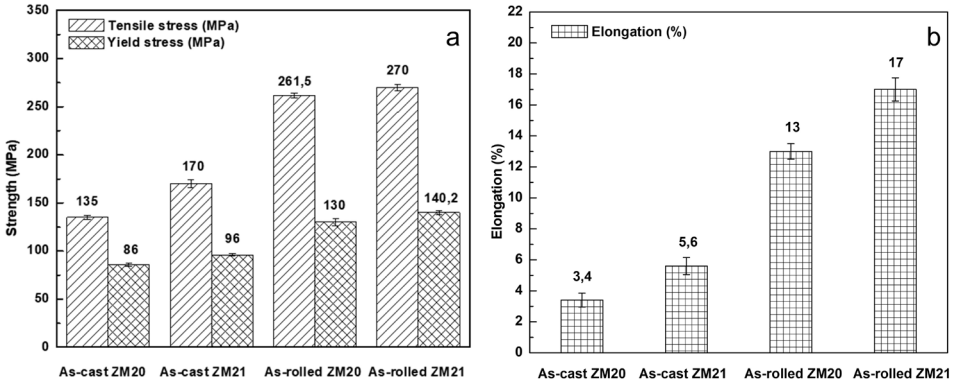

Fig. 5. Strength results of the alloys: (a) tensile and yield stress (MPa), (b) elongation (%)

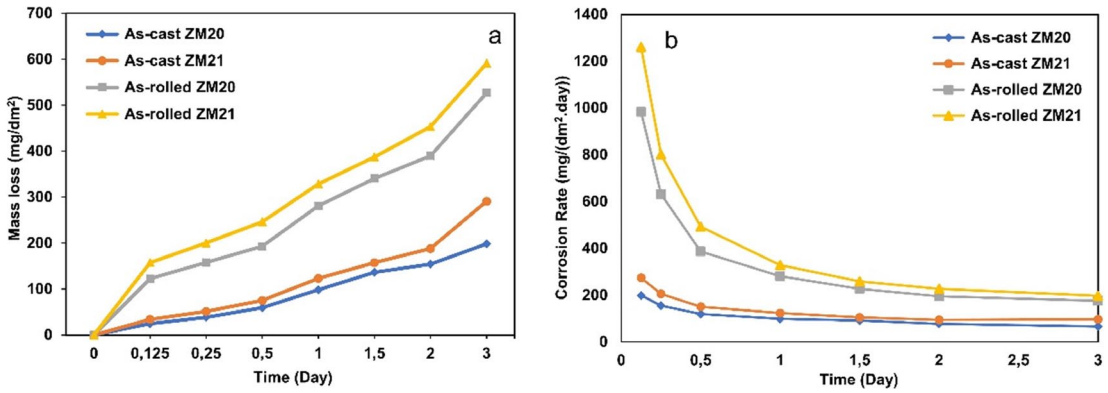

Fig. 6. Immersion test results of the alloys: (a) mass loss and (b) corrosion rate by time

the highest mass loss versus the given time, while the lowest mass loss was observed in the as-cast ZM20 alloy. Corrosion rates in units of (mg/(dm^2.day)) determined for each time are given in Fig. 6(b). Corrosion rate changing became stable at the end of 3 days, and the corrosion rate values determined for 3 days are called steady state corrosion rate.

The change of the steady state corrosion rate according to grain size is given in Fig. 7. As seen in Fig. 7, it was observed that the steady state corrosion rates of the ZM20 and ZM21 alloys after casting and rolling increased gradually based on the grain size.

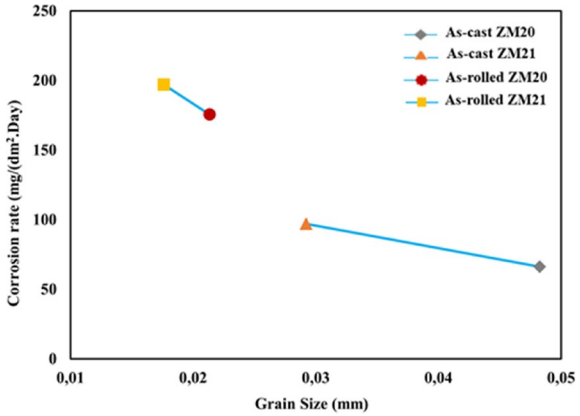

Fig. 7. Relationship between grain size and the steady state corrosion rate after the immersion test

J. Kubásek and D. Vojtěch [14] reported that zinc (1 and 3 wt.%) improves the corrosion resistance of as-cast Mg-based binary alloys. However, addition of Gd to Mg-3Zn alloys has strong detrimental effects on corrosion resistance because of the galvanic effect that occurs between the continuous network of the ternary phase and the magnesium matrix. S. Gollapudi reported in [16] that the decrease in corrosion resistance was attributed to the higher density of grain boundaries and other defects brought about by refinement.

SEM and EDX analyses after the immersion corrosion test are given in Fig. 8. As seen in Fig. 8, the corrosion mechanism has occurred in the form of wide-open and shallow pits. The concentration of the pits on the surface of the as-cast alloys increased with 0.51% Mn addition while the opened pits expanded to all surfaces with the homogenization and grain boundary corrosion were also observed in the as-rolled alloys. According to EDX analysis results, high oxygen content in the as-rolled alloys compared to that of the as-cast alloys shows the increase in corrosion.

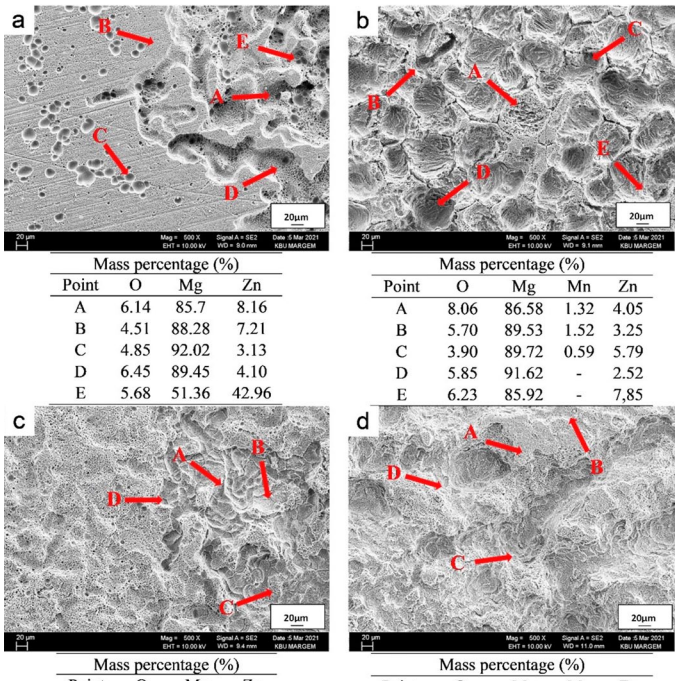

Mass percentage (%)

Point	O	Mg	Zn
A	6.14	85.7	8.16
B	4.51	88.28	7.21
C	4.85	92.02	3.13
D	6.45	89.45	4.10
E	5.68	51.36	42.96

Mass percentage (%)

Point	O	Mg	Mn	Zn
A	8.06	86.58	1.32	4.05
B	5.70	89.53	1.52	3.25
C	3.90	89.72	0.59	5.79
D	5.85	91.62	-	2.52
E	6.23	85.92	-	7,85

Mass percentage (%)

Point	O	Mg	Zn
A	7.80	87.23	4.98
B	4.95	90.74	4.30
C	6.99	88.02	4.99
D	7.81	86.57	5.62

Mass percentage (%)

Point	O	Mg	Mn	Zn
A	7.46	86.95	0.44	5.15
B	10.22	83.55	0.84	5.39
C	18.84	76.83	-	4.33
D	7.22	87.54	0.06	5.19

Fig. 8. EDX results of sample after immersion test: (a) as-cast ZM20, (b) as-cast ZM21, (c) as-rolled ZM20 and (d) as-rolled ZM21

3.5.2. Potentiodynamic polarization tests

Fig. 9(a) shows the polarization curves obtained as a result of the potentiodynamic polarization tests conducted after casting and rolling. As seen in Fig. 9(a), it was determined in the obtained polarization curves that the rolled alloys had more negative values than the cast alloys. The Figure also shows the corrosion

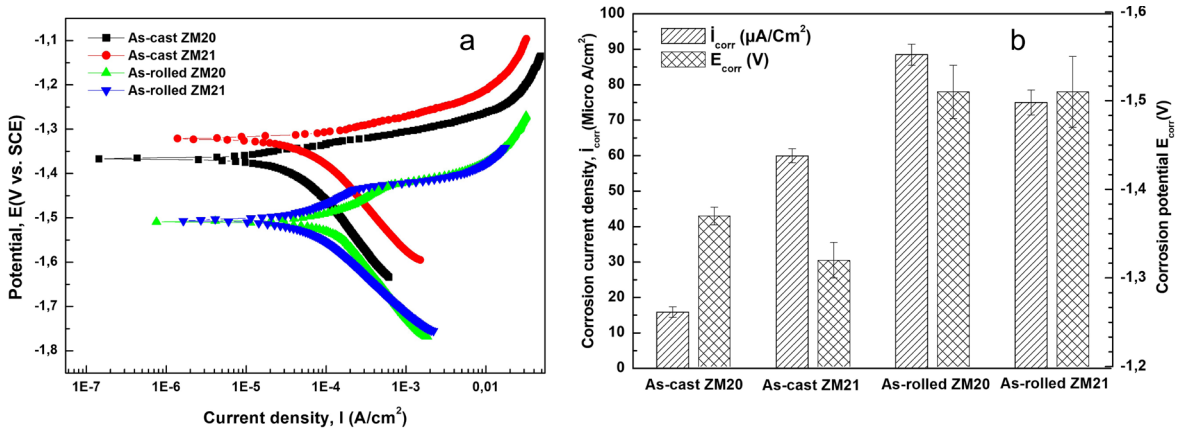

Fig. 9. Potentiodynamic corrosion test results (a) polarization curves, (b) corrosion current density and potential values of the as-cast and as-rolled alloys

current densities and corrosion potentials calculated from these. Looking at Fig. 9(b) and considering the corrosion potentials of the alloys after casting determined with the E_{corr} and i_{corr}, values, they had more positive values in comparison to the rolled alloys. The cast ZM21 alloy was more positive than the cast ZM20 alloy. The alloy with the lowest corrosion current density was the as-cast ZM20 alloy. The corrosion current density of the cast ZM21 alloy was higher, and its corrosion resistance was lower in comparison to the cast ZM20. The rolled ZM20 alloy had increased current density and reduced corrosion resistance in comparison to the cast ZM20 alloy. The rolled ZM21 alloy had slightly lower current density and slightly higher corrosion resistance than the cast ZM21 alloy. E. Zhang et al. [17] stated that the increasing of Zn content moved the corrosion potential E_{corr}, to a more negative direction and reduced the corrosion resistance. The noblest corrosion potential and the highest corrosion resistance were obtained for Mg-1Zn-Mn alloy.

3.5.3. Corrosive Wear test

The variation of the wear losses of the alloys in terms of (mg) examined in Fig. 10(a) and the specific wear rate coefficients calculated in terms of (mg/(N.m)), according to the sliding distance, are given in Fig. 10(b). According to Fig. 10, the change in weight loss with sliding distance is linear and at a given sliding distance the as-cast ZM20 exhibited the furthest weight loss while the as-rolled ZM21 showed the lowest weight loss. With increasing sliding distance, the variation of the specific wear rate coefficient of the as-cast alloys (Fig. 10(b)) decreases parabolically while that of the as-rolled alloys tend to be fixed with a slight increase towards the end of the sliding distance. The tendency of the specific wear rate coefficient sliding distance curve is expected to be parabolic decrease to some extent and then constant stable. With the increase in the sliding distance the specific wear rate coefficient of the as-rolled alloys is attributed to the more corrosion loss of these alloys and to increase further weight loss during friction. However, due to the high mechanical properties of the as-rolled alloys, the specific wear rate coefficient is lower than that of the as-cast alloys, making the as-rolled alloys more resistant to abrasion.

The variation of the specific wear rate coefficient with the grain size of the examined alloys is given in Fig. 11. Due to the improvement in the mechanical properties of the as-rolled alloys with refining grain size, the specific wear rate coefficients are lower than the as-cast alloys. In this study, the specific wear rate coefficients of both the as-cast and the as-rolled alloys added with 0,51 wt.% Mn are lowest since the grain size refinement

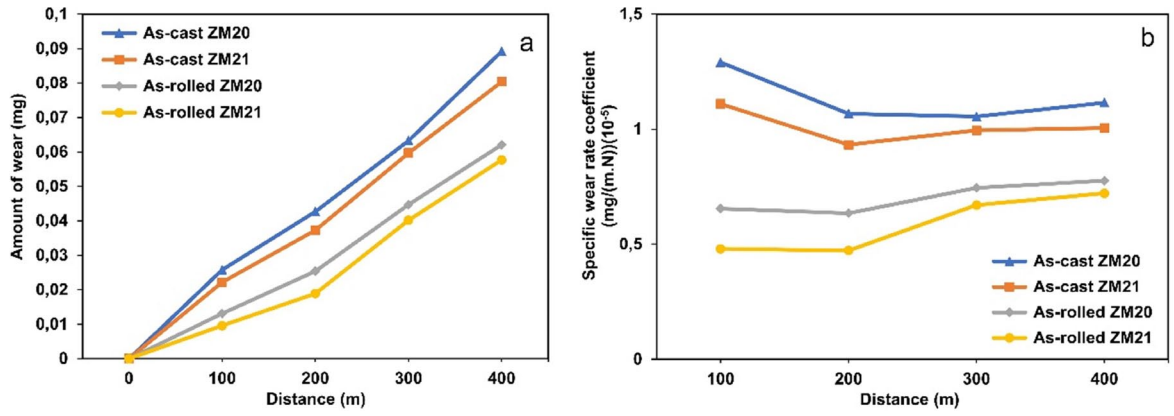

Fig. 10. Corrosive wear test results of the alloys: (a) amount of wear and (b) specific wear rate coefficient with sliding distance

is achieved with the addition of 0,51 wt.% Mn in the alloys produced by both as-rolled and as-cast conditions. H. li et al. [18] stated that the weight loss of Mg-Zn-Ca alloys decreased with increasing Zn content. With the increasing Zn content, the hardness of the alloy increased by the refining grain size, which led to the improvement of the wear resistance.

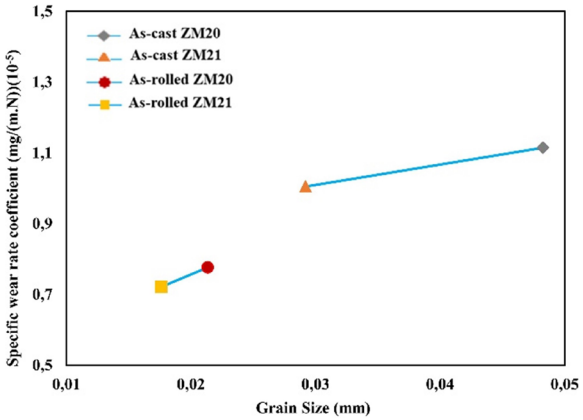

Fig.11. Relationship between grain size and the steady state specific wear rate coefficient after the corrosion wear test

In Fig. 12, the relationship between the friction coefficients and grain sizes of the alloys was shown and it was observed that the friction coefficient increased with the increase in the grain size with similar to Fig. 11.

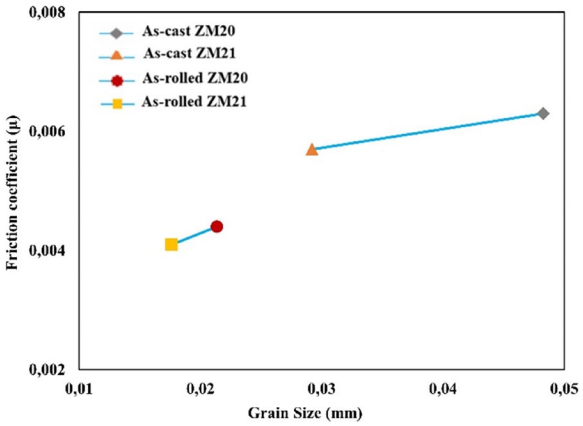

Fig. 12. Relationship between grain sizes and friction coefficients of the alloys after the corrosion wear test

SEM and EDX analyzes after the corrosion wear test are given in Fig. 13. As shown in Fig. 13, the increase in the white layer on the worn surface of the investigated alloys was revealed in the SEM images as parallel to the refining of the grains after rolling for both ZM20 and ZM21 alloys compared to the as-cast alloys. With the addition of 0,51 wt.% Mn to ZM20, this layer became more pronounced. In the as-rolled ZM21 alloy, which has the lowest friction coefficient, it is seen that this layer completely covers the surface. It has been observed that the increase of the oxide (white layer) plays an active role in the decrease of the friction coefficient. As determined in EDX analysis, the increase in these white layers with high oxygen content took an active role in the decrease of the friction coefficient.

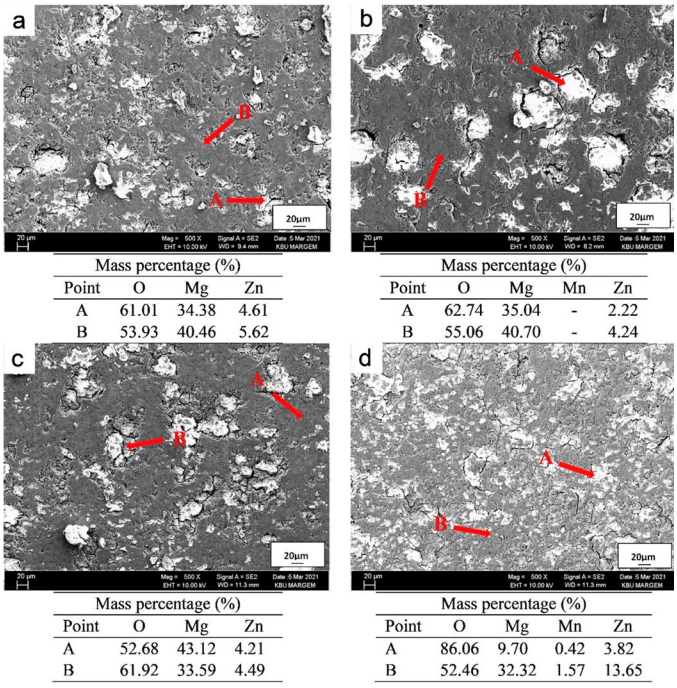

Mass percentage (%)

Point	O	Mg	Zn
A	61.01	34.38	4.61
B	53.93	40.46	5.62

Mass percentage (%)

Point	O	Mg	Mn	Zn
A	62.74	35.04	-	2.22
B	55.06	40.70	-	4.24

Mass percentage (%)

Point	O	Mg	Zn
A	52.68	43.12	4.21
B	61.92	33.59	4.49

Mass percentage (%)

Point	O	Mg	Mn	Zn
A	86.06	9.70	0.42	3.82
B	52.46	32.32	1.57	13.65

Fig. 13. EDX results of the investigated alloys after corrosive wear test: (a) as-cast ZM20, (b) as-cast ZM21, (c) as-rolled ZM20 and (d) as-rolled ZM21

4. Conclusions

The results of the comparing mechanical properties and corrosions behaviour of ZM20 (Mg-2wt.% Zn) and ZM21 (Mg-2wt.% Zn-0,51 wt.% Mn) alloys produced by both casting and rolling can be summarized as follows:

1. SEM, EDX and XRD results showed to be the MgZn, $MgZn_2$ and $MnZn_3$ binary phases in the microstructures of the investigated alloys.
2. In comparison to the other alloys, the as- rolled ZM21 alloy showed superior tensile, yield strength, elongation and hardness values due to a good combination of significant grain refining and dispersion resistance.
3. When the relationship between grain size and corrosion rate of the potentiodynamic and immersion corrosion test was examined, it was observed that the corrosion rate increased with the decrease in the grain size.
4. In the corrosive wear test, the specific wear rate coefficient increased depending on the grain size and white coloured oxide layer was seen formed substantially on the surface of the as-rolled ZM21 alloy in the SEM images.

Acknowledgement

This research is supported by the Scientific Research Projects of Karabuk University (BAP) with project no. FDK-2019-2103.

REFERENCES

[1] M.E. Mehtedi, L. Balloni, S. Spigarelli, E. Evangelista, G. Rosen, Hot workability and constitutive equations of ZM21 magnesium alloy, Key Eng. Mater. **367**, 79-86 (2008). DOI: https://doi.org/10.4028/www.scientific.net/KEM.367.79

[2] H.A. Gören, M. Ünal, E. Koç, A Comparative Study on Microstructure Properties of AZ91 Magnesium Alloy with Silicon Addition Using Ceramic Mold, Acta Physica Polonica A **135**, 5, 884-887 (2019). DOI: https://doi.org/10.12693/APhysPolA.135.884

[3] D.L. Atwell, M.R. Barnett, Extrusion limits of magnesium alloys, Metall. Mater. Trans. A **38A**, 12, 3032-3041 (2007). DOI: https://doi.org/10.1007/s11661-007-9323-2

[4] H. Zengin, Y. Turen, L. Elen, A Comparative Study on Microstructure, Mechanical and Tribological Properties of A4, AE41, AS41 and AJ41 Magnesium Alloys, J. of Materi. Eng. and Perform. **28**, 4647-4657 (2019). DOI: https://doi.org/10.1007/s11665-019-04223-8

[5] L. Elen, B. Cicek, E. Koc, Y. Turen, Y. Sun, H. Ahlatci, Effects of alloying element and cooling rate on properties of AM60 Mg alloy, Materials Research Express, 096511, 6 (9), 2053-1591, July (2019). DOI: https://doi.org/10.1088/2053-1591/ab2b13

[6] L.J. Liu, M. Schlesinger, Corrosion of magnesium and its alloys, Corros. Sci. **51**, 1733-1737 (2009). [CrossRef]. DOI: https://doi.org/10.1016/j.corsci.2009.04.025

[7] Q. Li, S. Fan, J. Peng, J. Yang, X. Jiang, F. Pan, Effects of Ce on microstructure and mechanical properties of ZM21 magnesium alloy, Materials Research Innovations **1**, sup. 4, S4-178-S4-182 (2014). DOI: https://doi.org/10.1179/1432891714Z.000000000662

[8] G. Mann, J.R. Griffiths, C.H. Cáceres, Hall-Petch parameters in tension and compression in cast Mg-2Zn alloys, Journal of Alloys and Compounds **378**, 188-191 (2004). DOI: https://doi.org/10.1016/j.jallcom.2003.12.052

[9] I.T. Caraballo, P.E.J.R.D.D. Castillo, Modelling and Design of Magnesium and High Entropy Alloys Through Combining Statistical and Physical Models. JOM **67**, 108-117 (2015). DOI: https://doi.org/10.1007/s11837-014-1242-2

[10] C.H. Caceres, G.E. Mann, J.R. Griffiths, Grain size hardening in Mg and Mg-Zn solid solutions, Metall. Mater. Trans. A **42**, 1950-1959 (2011). DOI: https://doi.org/10.1007/s11661-010-0599-2

[11] M. Thirumurugan, S. Kumaran, S. Suwas, T. Srinivasa Rao, Effect of rolling temperature and reduction in thickness on microstructure and mechanical properties of ZM21 magnesium alloy and its subsequent annealing treatment, Materials Science and Engineering: A **528**, 29-30, 15, 8460-8468, November (2011). DOI: https://doi.org/10.1016/j.msea.2011.07.047

[12] S. Gündüz, M.A. Erden, H. Karabulut, M. Türkmen, The Effect of Vanadium and Titanium on Mechanical Properties of Microalloyed PM Steel, Powder. Metall. Met. Ceram. **55**, 277-287 (2016). DOI: https://doi.org/10.1007/s11106-016-9803-2

[13] J. Yan, Z. Qin, K. Yan, Mechanical Properties and Microstructure Evolution of Mg-6 wt.% Zn Alloy during Equal-Channel Angular Pressing, Metals **8**, 10, 841 (2018). DOI: https://doi.org/10.3390/met8100841

[14] J. Kubásek, D. Vojtěch, Structural characteristics and corrosion behavior of biodegradable Mg-Zn, Mg-Zn-Gd alloys, J. Mater. Sci.: Mater. Med. **24**, 1615-1626 (2013). DOI: https://doi.org/10.1007/s10856-013-4916-3

[15] I.T. Caraballo, E.I.G. Nava, P.E.J.R.D.D. Castillo, Understanding the factors influencing yield strength on Mg alloys, Acta Materialia **75**, 287-296 (2014). DOI: https://doi.org/10.1016/j.actamat.2014.04.064

[16] S. Gollapudi, Grain size distribution effects on the corrosion behaviour of materials, Corrosion Science **62**, 90-94 (2012). DOI: https://doi.org/10.1016/j.corsci.2012.04.040

[17] E. Zhang, D. Yin, L. Xu, L. Yang, K. Yang, Microstructure, mechanical and corrosion properties and biocompatibility of Mg-Zn-Mn alloys for biomedical application, Materials Science and Engineering: C **29**, 3, 987-993 (2009). DOI: https://doi.org/10.1016/j.msec.2008.08.024

[18] H. Li, D. Liu, Y. Zhao, et al., The Influence of Zn Content on the Corrosion and Wear Performance of Mg-Zn-Ca Alloy in Simulated Body Fluid. J. of Materi. Eng. and Perform**. 25**, 3890-3895 (2016). DOI: https://doi.org/10.1007/s11665-016-2207-0